Multi-scale Ternary and Septenary Patterns for Texture classification

Rachdi El Mokhtar, Youssef El Merabet,, I. El Khadiri, Y Rhazi, C Meurie

Multi-scale Ternary and Septenary Patterns for Texture classification

E. Rachdi and Y. El merabet
dept. of physics,
Faculty of Sciences,
Ibn Tofail University
kenitra 14000, Morocco

I. El khadiri
Dept. of Algorithms
and Their Applications
Eötvös Loránd University
Budapest, Hungary
Department of physics,
Ibn Tofail University,
Kenitra, Morocco

Y. Rhazi
Electrical Engineering Department,
Faculty of Sciences and Technology,
Beni-Mellal, Morocco

C. Meurie
Univ Gustave Eiffel,
COSYS-LEOST, F-59650,
Villeneuve d'Ascq, France

***Abstract*—This paper proposes, inspired by local binary pattern (LBP) and its variants, a novel local texture operator for texture modelisation and classification, referred to as Multi-scale Ternary and Septenary Pattern (MTSP). MTSP is a histogram-based feature representation designed based on two single-scale STP and SSP encoders (single-scale ternary and septenary patterns, respectively). STP and SSP are built using a new set theory-based pattern encoding technique that combines the concpet of both LTP's and LQP's texture descriptors. The main idea behind STP and SSP is to calculate several virtual pixels based on different local and global image statistics and to progressively encode both local and non-local pixel interactions by analyzing the differential excitation and direction information based on the relationships between pixels sampled in different locations. Then, the obtained histograms of SSP and TSP methods are concatenated to form the final MTSP feature vector. Experiments have shown that MTSP has better performance stability across nine texture datasets than many recent state-of-the-art texture approaches.**

***Index Terms*—: Texture recognition, texture descriptors, LTP, LQP, LBP, directional topologies**

I. Introduction

In the field of texture analysis, texture classification over time is considered as a serious problem. It plays a very important role in many applications, such as image classification, facial classification, object recognition, gender classification, etc. However, textures in the real world vary in rotation, illumination, scale, and affine varieties when imaging conditions change. Extracting robust characteristics for texture modelisation remains a difficulty for texture analysis. Many improved methodologies for texture analysis have been developed in the literature over the years, with great evaluations found in [Liu et al., 2019]. Local feature extraction approaches have been remarkably designed and implemented in the area of texture analysis over the last decades. The main benefits of these local feature descriptors are that they are easy to implement and don't need a lot of training data [Bhattacharjee and Roy, 2019].

Among local feature extraction techniques, local binary patterns (LBP), established by [Ojala et al., 1996], is one of the most prominent texture descriptors among local feature extraction methods. Researchers regard LBP as a useful texture descriptor owing to its simplicity, good invariability to monotonic gray level changes, and applicability for real-time applications because of its low computational cost. Despite its origins in texture modeling and classification, the LBP approach has proven to be useful in a wide range of applications, including medical and biomedical image analysis, motion detection, image retrieval, face and facial description and identification, background removal, and more. Yet, the basic LBP descriptor has several drawbacks [El Merabet and Ruichek, 2018]. Therefore, in the past few years, many methods similar to LBP have been proposed to get around these problems and improve texture classification performance. Indeed, many dense-based feature extraction (LBP-based methods) continue to be designed still today, such as, Global refined local binary pattern (GRLBP) [Shu et al., 2022], Locally encoded transform feature histogram for rotation-invariant (LETRIST) [Song et al., 2017], Petersen graph multi-orientation based multi-scale ternary pattern (PGMO-MSTP) [El Khadiri et al., 2021], Circumferential local ternary pattern (CLTP) [Zheng et al., 2022], Local ternary pattern based multi-directional guided mixed mask (MDGMM-LTP) [El Khadiri et al., 2022], Oriented star sampling structure based multi-scale ternary pattern (O3S-MTP) [El Khadiri et al., 2020], Directional neighborhood topologies based multi-scale quinary pattern (DNT-MQP) [Rachdi et al., 2020], etc.

Even though LBP and its modifications achieve excellent performance, there needs to be a different way to improve the discriminative strength of an image so that modeling texture can be done more efficiently. Therefore, in this paper, we develop a conceptually and computationally simple yet powerful texture operator, named multi-scale ternary and septenary patterns (MTSP), for image texture understanding and analysis to better address the limitations of local feature descriptors. The MTSP technique computes feature representation by utilizing distinct neighborhood topologies to gather complete spatial information from neighboring pixels in various directions and blocks and describes the spatial connection and appearance of a particular pixel intensity. The MTSP operator is made up of two single-scale descriptors, STP (Single-scale Ternary

Pattern) and SSP (Single-scale Septenary Pattern) operators. A compact encoding scheme based on set theory is used to get feature maps. This scheme combines LQP and LTP-like texture methods to get more useful texture information.

The rest of this paper is organized as follows: In Section II, the basic local binary patterns (LBP) method is briefly explained. In Section III, the proposed MTSP texture descriptor is explained in detail. Section IV provides comprehensive experimentation and comparative evaluation. Section V provides a summary of the findings and some suggestions for further research.

II. Brief Review of Basic Local Binary Patterns

The well-known texture operator LBP was first developed by Ojala et al. [Ojala et al., 1996], and it has since been shown to be a very efficient and computationally straightforward texture descriptor for monochromatic images, as illustrated in Figure 1. The LBP code is calculated for each pixel in the input image by comparing its intensity value to the intensities of its neighboring pixels in each 3×3 gray-scale image patch. In formal terms, the LBP label of a pixel a_c in the center of a 3×3 grid is formed using the kernel function LBP(.) (cf. Eq. 1).

$$LBP(a_c) = \sum_{p=0}^{P-1} \psi(a_p - a_c)2^p \tag{1}$$

where a_c is the central pixel, $a_{p;p\in\{0,1,\ldots,P-1\}}$ are its neighboring pixels and P corresponds to the number of neighboring pixels. $\psi(.)$ is the Heaviside step function defined as follow:

$$\psi(\mathrm{x}) = \begin{cases} 1 & \text{if } \mathrm{x} \geq 0, \\ 0 & \text{otherwise} \end{cases} \tag{2}$$

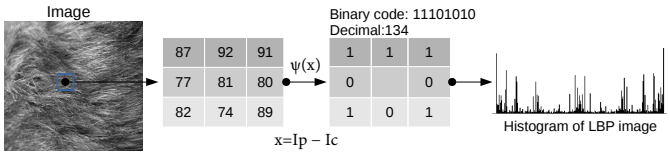

Fig. 1. Standard procedures for extracting LBP-like features.

III. Multi-Scale Ternary and Septenary Patterns (MTSP)

By combining and integrating the principles of LTP-like and LQP-like texture operators into the same compact encoding method, MTSP gains greater accuracy in texture modeling, leading to more promising results. The essence of MTSP is to locally sampling and encoding patterns in the most relevant directions of texture images. The MTSP descriptor is built by the following procedures:

A. Pattern sampling

The neighborhood topologies employed in MTSP take use of several intriguing aspects that may aid in performance enhancement depending on the following steps:

- take more pixels in the neighborhood to capture multi-scale objects;
- use blocks of pixels in several directions;
- use the average values and the median values of the surrounding blocks.

Several mean and median values (see the formulae presented below) are integrated as virtual pixels in the modeling of proposed texture patterns in order to increase the tolerances of the threshold ranges to identify a code insensitive to noise and more robust to illumination fluctuations. In order to do this, we look at the effects of different neighborhood layouts by direction and by block, as shown in Figures 2 and 3. From these figures, we get the following equations:

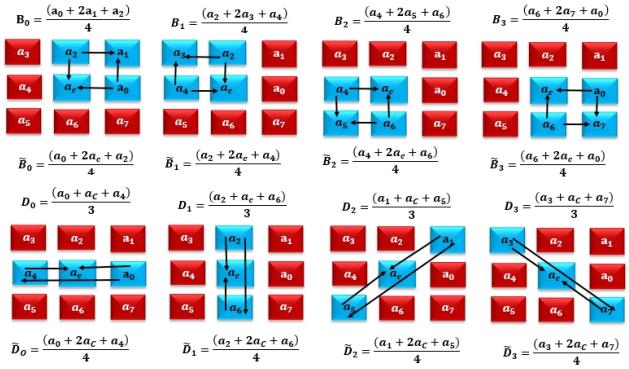

Fig. 2. Semantic representation for different template-directional neighborhood topologies.

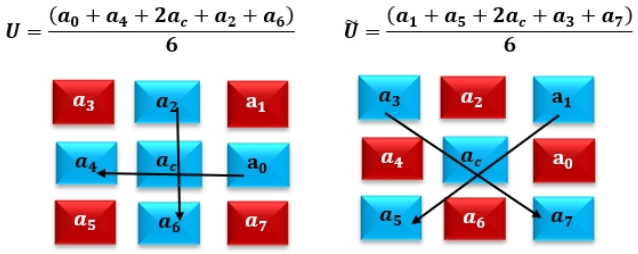

Fig. 3. Emantic representation for different template-block neighborhood topologies.

- **Direction** $\frac{k\pi}{4}$:

$$D_k = (a_k + a_c + a_{k+4})/3 \tag{3}$$

$$\widetilde{D}_k = (a_k + 2a_c + a_{k+4})/4 \tag{4}$$

Where D_k and $\widetilde{D}_k$ represent respectively the averages of (a_k, a_c, a_{k+4}) and (a_k, a_c),(a_c, a_{k+4}) respectively, where $k \in \{0, 1, 2, 3\}$, as presented in Figure 2.

$$U = (a_0 + a_4 + 2a_c + a_2 + a_6)/6 \tag{5}$$

$$\widetilde{U} = (a_1 + a_5 + 2a_c + a_3 + a_7)/6 \tag{6}$$

Where U and $\widetilde{U}$, represents the average value of the average intensities of the pixels of the directions $\pi/2$ & 0 including the central pixel and the average value of the intensities of the pixels of the directions $3\pi/4$ & $\pi/4$ including the central pixel, as presented in Figure 3.

- **Blocks delimited by the angles:** ($\frac{k\pi}{2}$, $\widehat{a_c}$, $\frac{(2k+1)\pi}{2}$)

$$B_k = (a_{2k} + 2a_{2k+1} + a_{2k+2})/4 \tag{7}$$

$$\widetilde{B}_k = (a_{2k} + 2a_c + a_{2k+2})/4 \tag{8}$$

Where B_k and $\widetilde{B}_k$, represent respectively the mean of $((a_{2k}, a_{2k+1}), (a_{2k+1}, a_{2k+2}))$ and the mean of $((a_{2k}, a_c), (a_c, a_{2k+2})$, where $k \in \{0, 1, 2, 3\}$

Then, we consider $(D_k$, $\widetilde{D}_k)$ and $(B_k$, $\widetilde{B}_k))$ as virtual neighboring pixels of the central pixel a_c, and then compute their local average and medians as shown in the following equations:

$$m_D = \frac{1}{9}(a_c + \sum_{k=0}^{3}(D_k + \widetilde{D}k)) \tag{9}$$

$$m_B = \frac{1}{9}(a_c + \sum_{k=0}^{3}(B_k + \widetilde{B}_k)) \tag{10}$$

$$\widetilde{M_I} = \frac{1}{M \times N}(\sum_{i=0}^{M-1}\sum_{j=0}^{N-1}(a_{i,j})) \tag{11}$$

$$\widetilde{m}_D = median(D) \tag{12}$$

$$\widetilde{m}_B = median(B) \tag{13}$$

$$\widetilde{M_I} = median(I_{M\times N}) \tag{14}$$

by considering the virtual pixels, the neighbouring pixels as well as their median and average values, we construct six sampling sets denoted as $\mathfrak{F}_i$:

$$\mathfrak{F}_1 = \{D_0, D1, a_4, a_5, a_6, a_7\} \tag{15}$$

$$\mathfrak{F}_2 = \{D_2, D3, a_0, a_1, a_2, a_3\} \tag{16}$$

$$\mathfrak{F}_3 = \{M_I, U, a_1, a_3, a_5, a_7\} \tag{17}$$

$$\mathfrak{F}_4 = \{\tilde{M}_I, \tilde{U}, \tilde{B}_k\} \tag{18}$$

Avec $k \in \{0, ..., , 3\}$

$$\mathfrak{F}_5 = \{\frac{min(m_D, m_B)}{2}, \frac{min(\tilde{m}_D, \tilde{m}_B)}{2}, min(\tilde{D}_k, \tilde{B}_k)\} \tag{19}$$

Avec $k \in \{0, ..., , 3\}$

$$\mathfrak{F}_6 = \{\frac{max(m_D, m_B)}{2}, \frac{max(\tilde{m}_D, \tilde{m}_B)}{2}, max(\tilde{D}_k, \tilde{B}_k)\} \tag{20}$$

To get set operations, we use two kinds of Venn diagrams, i.e., Venn diagrams in upper and lower modes, as illustrated in Figures 4 and 5, respectively.

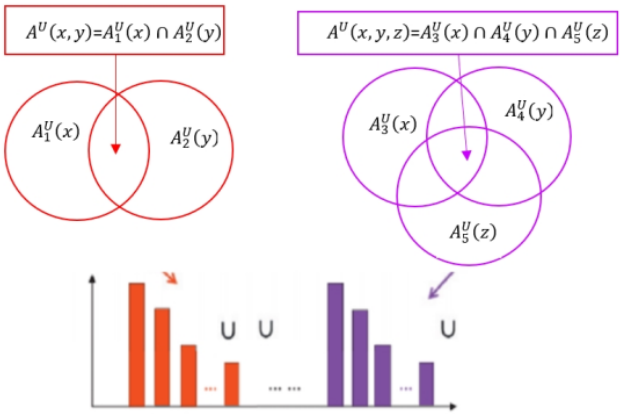

Fig. 4. A schematic image of the upper Venn diagrams mode .

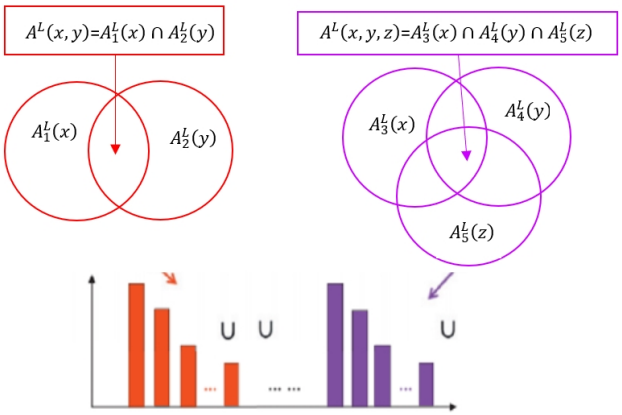

Fig. 5. A schematic image of the lower Venn diagrams mode .

Given the six sampling sets $\mathfrak{F}_k$, $k \in \{1, ..., 6\}$ defined above (cf. Eqs. (15) to (20)), an ansemble of sets of pixel relations are constructed based on three dynamic threshold values τ_1 , τ_2 and τ_3 according to the modes of the upper and lower Venn diagrams, as indicated in the following equations (cf. Eqs. 21) to (33)):

$$\mathbb{A}_1^U(x) = \{x \in \mathfrak{F}_1 \mid x \geq a_c - \tau_1\} \tag{21}$$

$$\mathbb{A}_2^U(x) = \{x \in \mathfrak{F}_2 \mid y \geq a_c + \tau_1\} \tag{22}$$

$$\mathbb{A}^U(x, y) = \mathbb{A}_1^U(x) \cap \mathbb{A}_2^U(y) \tag{23}$$

$$\mathbb{A}_1^L(x) = \{x \in \mathfrak{F}_1 \mid x \leq a_c + \tau_1\} \tag{24}$$

$$\mathbb{A}_2^L(x) = \{x \in \mathfrak{F}_2 \mid y \leq a_c - \tau_1\} \tag{25}$$

$$\mathbb{A}_3^U(x) = \{x \in \mathfrak{F}_3 \mid x \geq a_c + \tau_2\} \tag{26}$$

$$\mathbb{A}_4^U(x) = \{x \in \mathfrak{F}_4 \mid x \geq a_c - \tau_3\} \tag{27}$$

$$\mathbb{A}_5^U(x) = \{x \in \mathfrak{F}_5 \mid x \geq a_c + \tau_1\} \tag{28}$$

$$\mathbb{A}^U(x,y,z) = \mathbb{A}_3^U(x) \cap \mathbb{A}_4^U(y) \cap \mathbb{A}_5^U(z) \tag{29}$$

$$\mathbb{A}_3^L(x) = \{x \in \mathfrak{F}_3 \mid x \leq a_c - \tau_2\} \tag{30}$$

$$\mathbb{A}_4^L(x) = \{x \in \mathfrak{F}_4 \mid x \leq a_c + \tau_3\} \tag{31}$$

$$\mathbb{A}_5^L(x) = \{x \in \mathfrak{F}_6 \mid x \leq a_c - \tau_1\} \tag{32}$$

$$\mathbb{A}^L(x,y,z) = \mathbb{A}_3^L(x) \cap \mathbb{A}_4^L(y) \cap \mathbb{A}_5^L(z) \tag{33}$$

The local texture relationship between the the central pixel and each points within the considered six sampling sets $\mathfrak{F}_k$, $k \in \{1, ..., 6\}$, is encoded using three and seven-valued coding schemes (hence the name is ternary respectively septenary) according to the ensemble of sets of pixels relationship based on the three dynamic threshold values τ_1 , τ_2 and τ_3. To more precisely extract the entire micro-structural features included in these interconnections, we developed a texture operator named Multi-scale Ternary and Septenary Pattern (MTSP) which is conceptually comprised of Single-scale Ternary Pattern (STP) and Single-scale Septenary Pattern (SSP), as specified below:

1) Single-scale Ternary pattern (STP): Using a three-valued coding technique (i.e., the notion of LTP-like approaches), we created a Single-scale Ternary Pattern (STP) to encode the connection between the central pixel and the points of both sample sets $\mathfrak{F}_1$ and $\mathfrak{F}_2$. The indicator function $\phi(.)$ that transforms each pair connection into ternary form is defined as follows (cf. Eq. (42)):

$$\phi(\alpha) = \begin{cases} 1 & \text{if } \alpha \in \mathbb{A}^U(x,y), \\ 0 & \text{if } \alpha \in \mathbb{A}^U(x,y) \cap \mathbb{A}^L(x,y), \\ -1 & \text{if } \alpha \in \mathbb{A}^L(x,y). \end{cases} \tag{34}$$

The local information of the pixel a_c is then encoded using the STP encoder, expressed by the following equations (cf. Eq. (34) and (34)):

$$STP^{pattern}(a_c) = \sum_{p=0}^{5} \phi_{pattern}(a_c) \times 2^p \tag{35}$$

Where

$$\phi_{pattern}(x) = \begin{cases} 1 & \text{if } \phi(x) = \{1, 2\}, \\ 0 & \text{otherwise} \end{cases} \tag{36}$$

2) Single-scale Septenary Pattern (SSP): In the same way that LQP changed the LTP algorithm to work with the five-value encoding method, we use a seven-value encoding scheme based on three dynamic threshold values designed by [Rachdi et al., 2020], in order to represent the relationships between points in the rest of the sampling sets $\mathfrak{F}_k$; $k \in \{3, ..., 6\}$ and the central pixel. Furthermore, we can capture discriminant microstructure information from the perspective of the established ensemble of sets of pixels relationship using this method (i.e., Single-scale Septenary pattern (SSP)). SSP employs the following indicator denoted as $\psi(.)$ (cf. Eq. 37):

$$\psi(\alpha) = \begin{cases} +3 & \text{if } \alpha \in \mathbb{A}_3^U(x) \cap \mathbb{A}_4^U(y) \cap \overline{\mathbb{A}}^U(x,y,z), \\ +2 & \text{if } \alpha \in \mathbb{A}_4^U(x) \cap \mathbb{A}_5^U(y) \cap \overline{\mathbb{A}}^U(x,y,z), \\ +1 & \text{if} \alpha \in \mathbb{A}_3^U(x) \cap \mathbb{A}_5^U(y) \cap \overline{\mathbb{A}}^U(x,y,z), \\ -1 & \text{if } \alpha \in \mathbb{A}_3^L(x) \cap \mathbb{A}_5^L(y) \cap \overline{\mathbb{A}}^L(x,y,z), \\ -2 & \text{if } \alpha \in \mathbb{A}_4^L(x) \cap \mathbb{A}_5^L(y) \cap \overline{\mathbb{A}}^L(x,y,z), \\ -3 & \text{if } \alpha \in \mathbb{A}_3^L(x) \cap \mathbb{A}_4^L(y) \cap \overline{\mathbb{A}}^L(x,y,z), \\ 0 & \text{otherwise} \end{cases} \tag{37}$$

where $\overline{\mathbb{A}}^U$ designates the complement of $\mathbb{A}^U$.

Using the following SSP encoder , the local information of the pixels a_c is encoded as follows:

$$SSP^{pattern}(p,q) = \sum_{p=0}^{5} \psi_{pattern}(a_p) \times 2^p \tag{38}$$

Where $pattern \in \{1, 2, 3, 4, 5, 6\}$ represents six binary patterns by considering its upper-positive, middle-positive, lower-positive, upper-negative, middle-negative and lower-negative components denoted as $\psi(+3)$, $\psi(+2)$, $\psi(+1)$, $\psi(-1)$, $\psi(-2)$ and $\psi(-3)$ respectively. Note that SSP encodes an image in seven channels but gives six bit patterns. The image encoded by SSP is divided into six bit patterns under the following conditions:

$$\psi_{pattern}(x) = \begin{cases} 1 & \text{si } \psi(x) = \{1, 2, 3, 4, 5, 6\}, \\ 0 & \text{si } sinon. \end{cases} \tag{39}$$

B. Features extraction

After encoding each pixel in the input texture image using STP and SSP encoders, two feature maps are created. The following equations are used to convert the two feature maps into the texture-representing histograms.

$$h_{STP}(k) = \sum_{p=0}^{P-1} \widehat{\delta}(STP(a_p), k) \tag{40}$$

$$h_{SSP}(k) = \sum_{p=0}^{P-1} \widehat{\delta}(SSP(a_p), k) \tag{41}$$

where $k \in [0; 2^6]$ is the number of STP and SSP patterns. $\widehat{\delta}(.,.)$ denotes the Kronecker delta function defined as below:

$$\widehat{\delta}(x,y) = \begin{cases} 1 & \text{si } x = y, \\ 0 & \text{si } sinon. \end{cases} \tag{42}$$

Since several texture features provide various levels of descriptive power, combining them into a single row vector

feature seems to be the most effective strategy for making use of their combined strengths. A new hybrid texture description model is created via the use of a multi-scale fusion operation to achieve this goal and capture more prominent texture properties. By combining the STP and SSP operators, they generate the multi-scale ternary and septenary pattern (MTSP) (cf. Eq. 43), which is considered to be more effective due to the fact that it improves the discriminatory and expressive capabilities of both original operators.

$$h(MTSP) = \left\langle h_{STP}, h_{SSP}, \right\rangle \tag{43}$$

where $\langle . \rangle$ is the concatenation operator of the two histograms h_{STP} et h_{SSP}

IV. EXPERIMENTAL RESULTS AND DISCUSSION

In this section, the proposed MTSP descriptor's efficiency and performance were tested on several publicly available texture and material datasets (cf. Figure 6) and compared to 15 recent state-of-the-art feature extraction methods using a set of experiments. The experiments here used the split-sample validation protocol, in which half of the images are selected randomly for training and the other half are used for testing. In addition, the classification task is carried out using the parameter-free nearest-neighbor classifier (1-NN) with the L1-city block distance. Note that the classification tasks are repeated over 100 random splits to avoid any bias associated with the data partitioning and that the average results are used to measure the final accuracy. Table I depict the feature extraction methods tested and compared with the proposed descriptor.

N	Texture descriptor	Reference
1	Local binary patterns (LBP)	[Ojala et al., 1996]
2	Local ternary patterns (LTP)	[Tan and Triggs, 2010]
3	Local binary patterns (LQP)	[Nanni et al., 2010]
4	Improved local texture patterns (ILTP)	[Yang and Sun, 2011]
5	Median robust extended local binary pattern (MRELBP)	[Liu et al., 2016]
6	Locally encoded transform feature histogram (LETRIST)	[Song et al., 2017]
7	Repulsive-and-attractive local binary gradient contours (RALBGC)	[El Khadiri et al., 2018b]
8	Local concave-and-convex micro-structure patterns (LCCMSP)	[El Merabet and Ruichek, 2018]
9	Local directional ternary pattern (LDTP)	[El Khadiri et al., 2018a]
10	Mixed neighborhood topology cross decoded patterns (MNTCDP)	[Kas et al., 2018]
11	improved local Quinary patterns (ILQP)	[Armi and Fekri-Ershad, 2019]
12	Attractive-and-repulsive center-symmetric LBP (ARCSLBP)	[El Merabet and Ruichek, 2019]
13	Directional neighborhood topologies based MQP (DNT-MQP)	[Rachdi et al., 2020]
14	Local triangular coded pattern (LTCP)	[Arya and Vimina, 2021]
15	LTP based multi-directional guided mixed mask (MDGMM-LTP)	[El Khadiri et al., 2022]

TABLE I
FEATURE EXTRACTION METHODS USED IN THIS EXPERIMENT.

A. Texture datasets

Extensive tests are conducted on nine popular datasets—BonnBTF, JerryWu, Brodatz, KTH-TIPS, KTH-TIPS2b, USPtex1, VisTex, MBT, and NewBarkTex—to validate MTSP's capabilities and performance stability. These datasets were chosen because they are representative of a range of factors, including the number of images and classes included, and the unique problems inherent to each dataset, as shown in Table 6.

N°	Name	Classes	Samples per class	Samples resolution	Image format
1	Jerry WU	29	4	256×256	Color (BMP)
2	Bon BTF	10	16	200×200	Color (JPEG)
3	Brodatz	13	16	256×256	Monochrome (TIFF)
4	KTH-TIPS	10	4	664×640	Monochrome (PNG)
5	KTH-TIPS2b	11	176	100×100	Color (PNG)
6	USPtex1.0	191	2292	128 × 128	Color (BMP)
7	MBT	154	2464	128×128	Color (BMP)
8	NewBarkTex	6	1632	64×64	Color (BMP)
9	VisTex	16	40	128×128	Color (BMP)

.

Fig. 6. Image datasets used in this study.

B. Comparative Assessment of Performance

1) Experiment #1: Investigation on Performance Stability:

The following conclusions may be drawn from Tables II and III, which summarize the classification accuracies achieved on average for each technique evaluated and the overall ranking for each dataset:

1) It can be seen that the Single-scale Ternary Pattern (STP), the Single-scale Septenary Pattern (SSP), and their combination (MSTP), tend to achieve the highest and most stable discriminative accuracy of all the methods tested.
2) The proposed MTSP operator achieved a maximum classification accuracy of 100% across four datasets (i.e., BonnBTF, JerryWu, Brodatz, and KTH-TIPS), indicating that our technique was able to distinguish between all classes flawlessly and offers no space for improvement. Note that our method was the only method to achieve 100% over 4 different datasets.
3) A further finding from Table II shows that none of the evaluated feature extraction methods performed well over all the tested datasets. In fact, our proposed method achieves the highest average accuracy over six datasets out of the nine tested ones, indicating that the MSTP method is more stable and strong than all the tested methods. Note that for the three remaining datasets, the proposed method keeps its strength by achieving an average accuracy that is competitive with the score provided by the top one method in each dataset, as illustrated in Columns 6, 8, and 9 in Table II. Using the USPtex1 dataset as an example (column 6 in Table II), the proposed method is ranked second with an average accuracy of 91.13%, which is a very good classification rate (close to the average accuracy of the top-ranked feature extraction method, DNT-MQP, which is 92.46%). The same finding is correct for the other two datasets.

Based on the observations outlined above, it is clear that MSTP consistently outperforms the state-of-the-art feature extraction approaches examined in our studies across the vast majority of the tested texture and material datasets.

Descriptors	BonnBTF	JerryWu	Brodatz	KTH-TIPS	KTH-TIPS2b	USPtex1.0	VisTex	MBT	NewBarkTex
MTSP	100	100	100	100	95.61	91.13	80.93	87.96	85.04
STP	99.51	99.33	99.98	100	92.28	86.28	79.35	88.60	77.53
SSP	99.96	99.83	99.95	100	93.86	89.93	77.68	83.57	81.76
DNT-MQP	99.25	99.88	100	100	95.12	92.46	78.22	86.91	86.98
LETRIST	100	100	99.99	100	90.08	89.34	68.68	81.39	63.12
LCCMSP	97.64	98.18	100	100	93.32	88.42	78.27	85.41	84.72
ARCSLBP	99.17	99.53	99.88	100	93.23	86.89	75.76	83.23	78.66
LDTP	99.88	98.23	100	100	90.47	83.00	76.76	82.97	72.66
ILQP	98.72	98.03	100	100	93.39	87.54	75.39	85.80	83.85
RALBGC	98.80	97.51	100	100	93.39	87.16	77.89	86.22	84.56
MDGMM-LTP	100	98.01	100	100	93.57	89.37	79.21	87.19	85.17
LBP	95.86	97.26	100	100	89.67	81.43	74.19	85.61	79.00
LTCP	98.59	97.74	100	100	88.14	80.44	72.78	84.42	76.56
ILTP	99.17	98.32	100	100	93.91	88.83	77.44	84.74	84.44
LTP	98.64	98.06	100	100	92.92	86.42	75.38	88.56	82.81
LQP	97.06	97.69	99.97	99.90	93.17	85.42	73.83	89.31	78.54
MRELBP	98.97	99.53	100	100	89.00	84.38	64.74	75.66	61.81
MNTCDP	100	100	100	100	90.93	85.73	79.53	78.95	71.03

TABLE II

THE ACHIEVED CLASSIFICATION PERFORMANCE OF STATE-OF-THE-ART FEATURE EXTRACTION TECHNIQUES.

BonnBTF	JerryWu	Brodatz	KTH-TIPS	KTH-TIPS2b	USPtex1.0	VisTex	MBT	NewBarkTex
MTSP(100%)	MTSP(100%)	MTSP(100%)	MTSP(100%)	MTSP(95.61%)	DNT-MQP(92.46%)	MTSP (80.93%)	LQP(89.31%)	DNT-MQP(86.98%)
LETRIST	LETRIST	DNT-MQP	STP(100.00 %)	DNT-MQP	MTSP	MNTCDP	STP(88.61 %)	MDGMMLTP
MNTCDP	MNTCDP	RALBGC	SSP(100.00 %)	ILTP	SSP(89.93 %)	STP(79.35%)	LTP	MTSP
MDGMMLTP	DNT-MQP	LDTP	DNT-MQP	SSP(93.86 %)	MDGMMLTP	MDGMMLTP	MTSP	RALBGC
SSP(99.51%)	SSP(99.96%)	ILQP	LETRIST	MDGMMLTP	LETRIST	RALBGC	MDGMMLTP	RALBGC
LDTP	RCSLBP	RALBGC	RALBGC	ILQP	ILTP	DNT-MQP	DNT-MQP	ILTP
STP(99.51 %)	MRELBP	MDGMMLTP	RCSLBP	RALBGC	RALBGC	RALBGC	RALBG	ILQP
DNT-MQP	STP(99.33%)	LBP	LDTP	RALBGC	ILQP	SSP(77.68 %)	ILQP	LTP
RALBGC	ILTP	LTCP	ILQP	RCSLBP	RALBGC	ILTP	LBP	SSP(81.76%)
ILTP	LDTP	ILTP	RALBGC	LQP	RCSLBP	LDTP	RALBGC	LBP
MRELBP	RALBGC	LTP	MDGMMLTP	LTP	LTP	RCSLBP	ILTP	RCSLBP
RALBGC	LTP	MRELBP	LBP	STP(92.28 %)	STP(86.28%)	ILQP	LTCP	LQP
ILQP	ILQP	MNTCDP	LTCP	MNTCDP	MNTCDP	LTP	SSP(83.57 %)	STP(77.53 %)
LTP	MDGMMLTP	LETRIST	ILTP	LDTP	LQP	LBP	RCSLB	LTCP
LTCP	LTCP	STP (99.98%)	LTP	LETRIST	MRELBP	LQP	LDTP	LDTP
RALBGC	LQP	LQP	MRELBP	LBP	LDTP	LTCP	LETRIST	MNTCDP
LQP	RALBGC	SSP(99.95%)	MNTCDP	MRELBP	LBP	LETRIST	MNTCDP	LETRIST
LBP	LBP	RCSLBP	LQP	LTCP	LTCP	MRELBP	MRELBP	MRELBP

TABLE III

ON EACH OF THE DATASETS EVALUATED, A RANKING OF THE FEATURE EXTRACTION TECHNIQUE RESULTS WAS PERFORMED. THE APPROACH PRESENTED IS INDICATED IN LIGHT GRAY.

2) Experiment #2: Statistical significance of the achieved results in terms of accuracy improvement:

The objective of this section is to further prove statistically the realized performances via MTSP compared to the existing evaluated methods by employing the Wilcoxon signed rank test-based ranking technique [El Merabet and Ruichek, 2018]. The algorithm is applied to all the pairwise combinations of the 18 evaluated methods, including (STP and SSP and their combination MTSP=STP+SSP) on the nine tested databases. Figure 7 depicts the achieved ranking results based on the normalized number of victories achieved by each method across all databases considered in our experiment. It is evident from the findings shown in Figure 7 that MSTP is the most effective operator among the most recent feature extraction techniques, validating the general conclusion drawn from Tables II and III.

Ranking 1NN	Texture descriptor	Victories/comparisons	Dimension	Reference
1	MTSP	0.70588	256	Proposed (2022)
2	DNT-MQP	0.62745	384	[Rachdi et al., 2020]
3	MDGMMLTP	0.51634	1022	[El Khadiri et al., 2022]
4	SSP	0.49673	128	Proposed (2022)
5	STP	0.45098	128	Proposed (2022)
6	ILTP	0.41830	1024	[Yang and Sun, 2011]
7	LCCMSP	0.37255	2046	[Ruichek et al., 2018]
8	RALBGC	0.36601	1022	[El Khadiri et al., 2018]
9	MNTCDP	0.36601	2048	[Kas et al., 2018]
10	LTP	0.33333	512	[Tan and Triggs, 2010]
11	ARCSLBP	0.32026	256	[Ruichek et al., 2019]
12	ILQP	0.32026	1024	[Armi and Fekri-Ershad, 2019]
13	LETRIST	0.31373	413	[Song et al., 2017]
14	LQP	0.25490	1024	[Nanni et al., 2010]
15	LDTP2	0.24183	1022	[Chahi et al., 2018]
16	LBP	0.15033	256	[Ojala et al., 1996]
17	MRELBP	0.12418	200	[Liu et al., 2016]
18	LTCP	0.11111	256	[Arya and Vimina, 2021]

Fig. 7. Ranking results and the number of victories obtained for the 18 evaluated methods.

V. CONCLUSION

In this paper, we introduce Multi-scale Ternary and Septenary Pattern (MTSP), an innovative feature extraction method that makes use of set theory, neighborhood topology, and multiple oriented blocks. In fact, MTSP encodes the linkages and interactions between pixels in a 3×3 grayscale image patch using a compact coding technique that combines the ideas of LTP and LQP-like technologies. The capabilities and performance stability of MTSP's were evaluated on nine complex texture databases using the 1-NN classifier against

15 new and advanced state-of-the-art texture operators. The MTSP descriptor performed well across all databases, both in terms of results and dimensions, indicating that it provides a more accurate representation of texture images. In future work, we plan to try out more advanced classifiers in order to improve classification accuracy.

REFERENCES

[Armi and Fekri-Ershad, 2019] Armi, L. and Fekri-Ershad, S. (2019). Texture image classification based on improved local quinary patterns. *Multimedia Tools and Applications*, 78(14):18995–19018.

[Arya and Vimina, 2021] Arya, R. and Vimina, E. (2021). Local triangular coded pattern: a texture descriptor for image classification. *IETE Journal of Research*, pages 1–12.

[Bhattacharjee and Roy, 2019] Bhattacharjee, D. and Roy, H. (2019). Pattern of local gravitational force (plgf): A novel local image descriptor. *IEEE transactions on pattern analysis and machine intelligence*, 43(2):595–607.

[El Khadiri et al., 2018a] El Khadiri, I., El Merabet, Y., Chahi, A., Ruichek, Y., Touahni, R., et al. (2018a). Local directional ternary pattern: A new texture descriptor for texture classification. *Computer vision and image understanding*, 169:14–27.

[El Khadiri et al., 2022] El Khadiri, I., El Merabet, Y., Ruichek, Y., Chetverikov, D., El Mokhtar, R., and Tarawneh, A. S. (2022). Local ternary pattern based multi-directional guided mixed mask (mdgmm-ltp) for texture and material classification. *Expert Systems with Applications*, page 117646.

[El Khadiri et al., 2020] El Khadiri, I., El Merabet, Y., Ruichek, Y., Chetverikov, D., Touahni, R., et al. (2020). O3s-mtp: Oriented star sampling structure based multi-scale ternary pattern for texture classification. *Signal Processing: Image Communication*, 84:115830.

[El Khadiri et al., 2021] El Khadiri, I., El Merabet, Y., Tarawneh, A. S., Ruichek, Y., Chetverikov, D., Touahni, R., and Hassanat, A. B. (2021). Petersen graph multi-orientation based multi-scale ternary pattern (pgmo-mstp): An efficient descriptor for texture and material recognition. *IEEE Transactions on Image Processing*, 30:4571–4586.

[El Khadiri et al., 2018b] El Khadiri, I., Kas, M., El Merabet, Y., Ruichek, Y., and Touahni, R. (2018b). Repulsive-and-attractive local binary gradient contours: New and efficient feature descriptors for texture classification. *Information Sciences*, 467:634–653.

[El Merabet and Ruichek, 2018] El Merabet, Y. and Ruichek, Y. (2018). Local concave-and-convex micro-structure patterns for texture classification. *Pattern Recognition*, 76:303–322.

[El Merabet and Ruichek, 2019] El Merabet, Y. and Ruichek, Y. (2019). Attractive-and-repulsive center-symmetric local binary patterns for texture classification. *Engineering Applications of Artificial Intelligence*, 78:158–172.

[Kas et al., 2018] Kas, M., Ruichek, Y., Messoussi, R., et al. (2018). Mixed neighborhood topology cross decoded patterns for image-based face recognition. *Expert Systems with Applications*, 114:119–142.

[Liu et al., 2019] Liu, L., Chen, J., Fieguth, P., Zhao, G., Chellappa, R., and Pietikäinen, M. (2019). From bow to cnn: Two decades of texture representation for texture classification. *International Journal of Computer Vision*, 127(1):74–109.

[Liu et al., 2016] Liu, L., Lao, S., Fieguth, P. W., Guo, Y., Wang, X., and Pietikäinen, M. (2016). Median robust extended local binary pattern for texture classification. *IEEE Transactions on Image Processing*, 25(3):1368–1381.

[Nanni et al., 2010] Nanni, L., Lumini, A., and Brahnam, S. (2010). Local binary patterns variants as texture descriptors for medical image analysis. *Artificial intelligence in medicine*, 49(2):117–125.

[Ojala et al., 1996] Ojala, T., Pietikäinen, M., and Harwood, D. (1996). A comparative study of texture measures with classification based on featured distributions. *Pattern recognition*, 29(1):51–59.

[Rachdi et al., 2020] Rachdi, E., El Merabet, Y., Akhtar, Z., and Messoussi, R. (2020). Directional neighborhood topologies based multi-scale quinary pattern for texture classification. *IEEE Access*, 8:212233–212246.

[Shu et al., 2022] Shu, X., Pan, H., Shi, J., Song, X., and Wu, X.-J. (2022). Using global information to refine local patterns for texture representation and classification. *Pattern Recognition*, 131:108843.

[Song et al., 2017] Song, T., Li, H., Meng, F., Wu, Q., and Cai, J. (2017). Letrist: Locally encoded transform feature histogram for rotation-invariant texture classification. *IEEE Transactions on circuits and systems for video technology*, 28(7):1565–1579.

[Tan and Triggs, 2010] Tan, X. and Triggs, B. (2010). Enhanced local texture feature sets for face recognition under difficult lighting conditions. *IEEE transactions on image processing*, 19(6):1635–1650.

[Yang and Sun, 2011] Yang, W. and Sun, C. (2011). Face recognition using improved local texture patterns. In *2011 9th World Congress on Intelligent Control and Automation*, pages 48–51. IEEE.

[Zheng et al., 2022] Zheng, Z., Xu, B., Ju, J., Guo, Z., You, C., Lei, Q., and Zhang, Q. (2022). Circumferential local ternary pattern: New and efficient feature descriptors for anti-counterfeiting pattern identification. *IEEE Transactions on Information Forensics and Security*, 17:970–981.